Numerical modelling of infiltration of Al into additive manufactured Fe preforms in order to obtain Fe-Al intermetallics

IOP Conf. Series: Materials Science and Engineering **529** (2019) 012014 doi:10.1088/1757-899X/529/1/012014

Numerical modelling of infiltration of Al into additive manufactured Fe preforms in order to obtain Fe-Al intermetallics

R. Berger[1,a], S. Jana[1], N. Focks[1], H. Michels[1], W. Kochanek[2], C. Charitidis[3]

1: Access e.V., Intzestraße 5, 52072 Aachen, Germany
2: Dr.Wolfgang Kochanek Ent., Freiheitstr. 57, 67434 Neustadt, Germany
3: NTUA, 9 Heroon Polytechniou St., Zographos, Athens, Greece GR-157 73
a: Corresponding Author: R. Berger - Email: r.berger@access-technology.de

Abstract. The current work, describes a numerical methodology to obtain deeper understanding of the kinetics of solidification and the dynamics of Al melt infiltration into porous iron preforms, in order to develop a near net shape process for a new class of highly advanced ductile and fine grained Fe-Al intermetallic. Investigations on macroscale simulations revealed that certain pressure and wetting conditions are beneficial for infiltration into finer structures. Microstructure showed a dependency of the solidification process on diffusion. Estimates for infiltration and solidification times are developed to determine which structures can be infiltrated before solidification stops melt flow.

1. Introduction and objectives of the work

Chromium and Nickel are listed in the table of Critical Raw Materials (CRMs) with a current projected lifetime of 25 – 100 Years [1-3]. In line with the strategy to find solutions to replace these CRMs in high volume end consumer products, a HORIZON-2020 project: EQUINOX [4] was funded to develop a novel process that allows to substitute Cr/Ni based (stainless) steel parts used in certain consumer products. The goals of this technological development is to develop a novel near net shape process for a new class of highly advanced ductile and fine grained Fe-Al based intermetallics. The basis of this development will be based on a reactive infiltration process of porous iron preforms with liquid Al or an Al-Fe-alloy, by using two different pressure assisted techniques: suction and centrifugal casting. Fine grain structures, which benefit tensile strength and ductility [5], are achieved by infiltrating preforms with fine structured porosity. Infiltration of Al in porous preforms can also be used for rapid prototyping [6]. Here the permeability of additive manufactured materials has a major impact on the infiltration process, but it is also important e.g. in biomedicine applications [7,8].

The first step is to effectively infiltrate melt into the preforms, which is directly related to the melt flow paths, or the structure of porosity in these preforms. Different preforms were manufactured by selective laser melting process (SLM), Metal injection Moulding (MIM), Powder metallurgy moulding and sintering (PMM) and Kochanek Process (KE) [9]. Preforms from SLM process consists of Fe-powder and characterized by thin long roughly square channels of approximately 400 -550 µm in size, representing around 50% of porosity. The unique process of manufacturing preforms developed by [9] uses powder moulding process of metal oxides rather than pure metal powders.

The flexibility of the KE process allows building preforms of different porosities and channels of different sizes. For all industrial purposes, the KE process is highly viable cost effective compared to

SLM and other processes to manufacture preforms. However, the preforms from well controlled SLM process can be used to develop the manufacturing of preforms through KE process.

Initial centrifugal casting experiments performed at Access e.V. indicated well designed channels in SLM preforms are very effective for infiltration into the depths of a preform body (see Fig. 1). This aspect of development is currently explored within the EQUINOX project, to yield similar channels as those of SLM and with that a substantial improvement in infiltration depth.

Due to the complexity of the process multiscale modeling tools are being employed to guide the experiments. In this work, a simulation methodology based on computational fluid dynamics macroscopic simulations using STAR-CCM+[10] and microstructure simulations using MICRESS [11] is presented to obtain deeper understanding of the kinetics of solidification, the formation of intermetallic phases and the dynamics of Al melt infiltration into porous iron preforms, that will aid in design of channels in preform.

The structure of the paper is as follows: Section 2 presents modelling of infiltration and solidification. Section 3 summarizes the results for infiltration and solidification times. Section 4: concludes and summarizes the work.

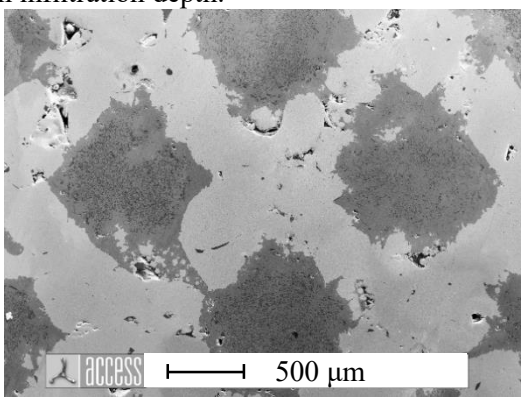

Figure 1: A metallographic image of a section of SLM sample after infiltration with Al.

2. Modelling and Simulation

2.1. Macrosimulation

Macrosimulations under isothermal conditions were performed to understand infiltration dynamics in these preforms. In the simulations two phases were considered, starting with gas filled preforms and variations considering surface tension, and contact angle effects, viscosity, pressure etc., were included in order to understand how these parameters affect filling of these preforms consisting of inlay channels.

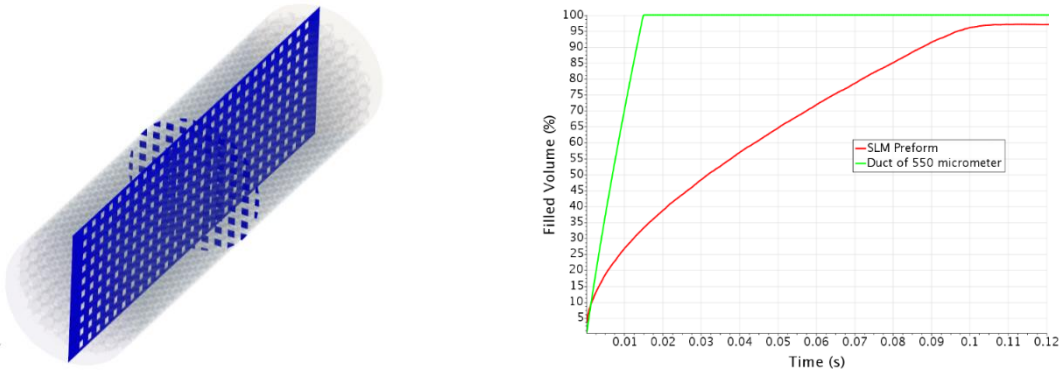

Figure 2: Left: Snapshot of CAD model of SLM manufactured preform (transparent view shows the entire geometry with internal structure, and cross-sections are shown in blue). **Right**: Comparison of filled volume of SLM preform (shown in Fig 1) and a simplified duct of 550 µm with inlet pressure of 20000 Pa, Surface tension coefficient of 0.9 N/m and wetting angle of 110°.

At first fluid flow in the centrifugal casting machine was simulated to obtain the typical melt pressure acting on the preform. This was obtained to be around 20000 Pa, which was used as inlet boundary conditions for subsequent investigations. Next filling simulations were then performed on an SLM preform (see Fig. 1) with an inlay channels of size of 550 µm and 40mm in length and a comparison of filling times are shown in Figure 2.

Simulations were performed on different square cross-section channel sizes, with a constant length of 4 cm. Results are shown in Table 1. A typical simulation setup consists of a square channel with inlet and outlet. At the inlet a boundary condition with a definite pressure is applied. All other boundaries are considered as walls with no slip boundary condition. The channel is assumed to be filled with air initially. Starting at simulation time t= 0 s, the melt is allowed to flow in with a pressure P = 20000 Pa. The simulations were performed using Al with 2700 Kg/m^3 density, 0.00125 Pa-s viscosity, 0.9 N/m Surface tension coefficient and the second medium was considered as air with 1.18415 Kg/m^3 density and 1.85x10^{-5} Pa·s viscosity. Initially the melt was assumed non-wetting (110° wetting angle) with the channel walls.

Table 1: Infiltration times for different square cross-section channel sizes and wetting angles.

No.	Channel Size (µm)	Wetting Angle (°)	Time for infiltration (s)	No.	Channel Size (µm)	Wetting Angle (°)	Time for infiltration (s)
1	550	110	0.01492	9	30	90	1.32
2	400	110	0.01842	10	30	80	0.655
3	200	110	0.056	11	10	90	8.8
4	100	110	0.354	12	10	80	2.51
5	100	90	0.145	13	3	90	Partial Infiltration
6	50	110	No Infiltration	14	3	80	6.8
7	50	100	1.4	15	1	90	Partial Infiltration
8	50	90	0.55	16	1	80	12

2.2. Thermodynamics

Prior to solidification simulations the thermodynamics of the Al-Fe system was investigated using the CALPHAD- (CALculation of PHAse Diagrams) software Thermocalc [12] and the High Entropy Alloys database [13]. Several solid phases occur in the Al-Fe system: The FCC aluminium phase, the intermetallic phases $Al_{13}Fe_4$, Al_5Fe_2, Al_2Fe and Al_5Fe_4, for low Al concentrations between 900°C and 1400°C FCC-iron (austenite) and a BCC-iron solid solution phase that can contain up to 50mol% Al. To account for the thermodynamics of phase transformations in the solidification simulations the phase field simulation is linked to the same thermodynamic database. Further details about the multiphase field model and the required material model parameters can be found in [14,15].

Because of its material properties the aim of the process is a material mainly consisting of the BCC-phase. In accordance with experimental work of Plevanchuk et al. [16] the average density of the Fe preform and the infiltrated Al melt is lower than the density of the intermetallic phase formed due to the reaction between the melt and the preform. This leads to volume shrinkage and thus porosity during the reaction. By infiltrating with an Al-Fe alloy instead of pure Al the above mentioned effects together with release of reaction heat are reduced or completely eliminated.

For this reason, and also to reduce formation of other intermetallic phases than the BCC phase infiltration with Al-Fe alloys of various compositions (25mol%, 33mol% and 50mol% Fe) was investigated in the solidification simulations.

2.3. Microsimulation

Phase field

Microstructure simulations were performed for solidification of melt filled SLM, PMM, MIM and KE preforms using the phase field method detailed in [17] and implemented in the software MICRESS [11]. Initial structures for the simulations were generated from CT-scans of the preforms. From these Representative Volume Elements (RVEs) were cut out and discretized on a regular grid. For SLM-structures an RVE of 400×400×250µm representing a quarter of a channel with surrounding material was discretized with a grid spacing of 2µm. For PMM-structures a region of 660×660×660µm was

discretized with 3mm grid spacing and for KE structures 10×10×10µm were discretized with 0.05µm spacing. Simulations for MIM-structures 2D simulations were done on a 25×50 µm grid with 0.1 µm spacing. In addition a series of 2D simulations was performed for channels with a square cross section and channel width varying from 1 µm to 400 µm. In these simulations a quarter of the channel and surrounding preform material (representing an initial solid fraction of 75% of the RVE) was discretized on a 200×200 grid. The initial structures for 3d simulations are shown in figure 3. To avoid the whole preform being represented by a single grain an artificial grain structure was superimposed on the solid region as shown in Figure 3.

At the start of the solidification simulations the pores were filled with melt, assuming completed infiltration. For KE- and MIM- structures this assumption is not realistic, since solidification blocks infiltration paths very fast for these fine structures and applicable infiltration pressure is limited to avoid structural damage of the preform. Nevertheless from simulations for these hypothetical conditions general trends for reaction times and permeabilities can be gained that are transferable to other structures and length scales. The starting temperatures were chosen to be about 20K above the liquidus temperature,

Initial melt composition and starting temperatures were: 25mol% Fe, 1450K (SLM 2D, SLM 3D, MIM, KE), 33mol% Fe, 1470K (PMM, KE) and 50mol% Fe 1610K (SLM 2D, square channel, MIM, KE). As thermal conditions for SLM- and PMM-structures heat extraction rates of 5, 10, 20 and 50 W/cm^3 were investigated. For the finer KE- and MIM-structures the reaction times are much shorter and exothermic heat release would drive temperatures up by 300K under the above process conditions. Under such conditions the initial microstructure of the preform would become quickly irrelevant due to coarsening, which would determine the features of the resulting structure. Thus for KE- and MIM-structures isothermal conditions were investigated, assuming coupling to a heat reservoir at constant temperature. For better comparability these conditions were also chosen for the square channel structures.

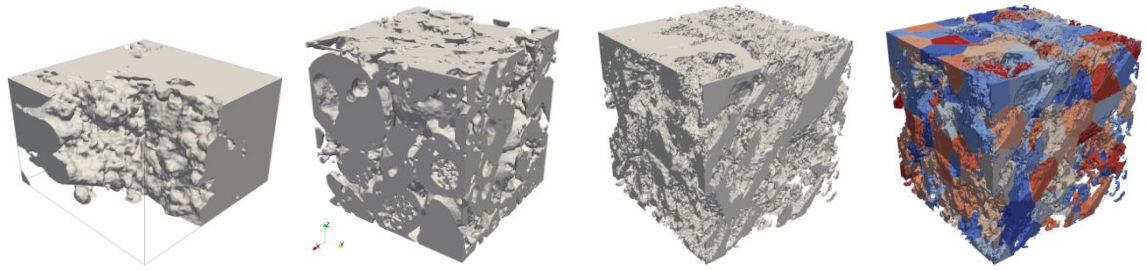

Figure 3: Initial RVEs. From left to right: SLM, PMM, KE, KE with superimposed grain structure.

Diffusivity

An important (and under isothermal conditions the only) contribution to the solidification in this process is the exchange of Fe for Al between BCC phase (i.e. preform) and melt, so that the Fe-enrichment raises the liquidus temperature. Thus the diffusivity in the BCC-phase plays an important role, since it determines how fast Fe is transported to and Al from the solid liquid interface. In all microstructure simulations the temperature dependency of the diffusivity in the BCC-Fe-phase is described by an Arrhenius law. Based on literature data [18] for various alloy compositions Q = 240 kJ/mol and D_0 = $2 \cdot 10^{-3}$ m^2/s were chosen as Arrhenius parameters. The resulting diffusivities are $D_{1450}=4.52\times10^{-12}$ m^2/s, $D_{1470}=5.92\times10^{-12}$ m^2/s and $D_{1610}=3.27\times10^{-11}$ m^2/s.

Results

The SLM, PMM, MIM and KE microstructures are very different, specifically with respect to the length scales. While in the SLM structures the length scale of the porosity is in the range of several hundred µm, in the PMM structures the diameters of pores and connecting channels are initially some 10 µm and in KE structures some 0.1 µm. The specific surface S_V (or its inverse) is chosen to quantify the length scale. It is defined as interfacial area (of the melt solid interface) per volume. The value of S_V was determined for the initial structures and tracked during the solidification.

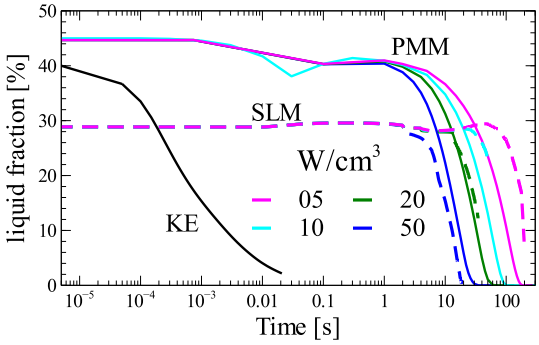

Figure 4: Solidification over time

The differences in length scale have a large impact on the time scale of the diffusion driven solidification and on the permeability as shown in figure 4. Compared are

- KE, infiltrated with Al33at%Fe with constant temperature condition (dotted, black)
- PMM, infiltrated with Al33at%Fe (solid lines) and
- SLM infiltrated with Al25at%Fe (dashed) at four cooling rates (see legend).

Figure 4 shows that in the fine KE structures it takes only several milliseconds for diffusion to increase the Fe-content in the melt, thereby solidifying it. For PMM structures solidification times vary from 30 to 190 s depending on the cooling rate, for SLM structures solidification takes over 200 s at the lowest cooling rate.

2.4. Analytic

To infiltrate an amount V_L of melt into a structure the energy $J_\sigma=\Delta\sigma\cdot S_L\cdot V_L$ is necessary in the non-wetting case to overcome surface tension. $\Delta\sigma$ is the difference between the interfacial energy of the free surface of the solid and the interfacial energy of the solid liquid interface and $S_L=S_V/f_L$ the surface per liquid volume. So a pressure $\Delta P_\sigma = J_\sigma/V_L = \Delta\sigma\cdot S_L$ is necessary to overcome surface tension during infiltration.

Additional pressure is needed to force the melt through the porous structure. For laminar flows this is described by the Darcy law that describes the dependency of the flux v_f (melt volume passing through an area per time and area) on the viscosity µ and a structure dependent permeability k. For the permeability k a simplified (approximating the tortuosity with 1) Carman-Kozeny rule can be applied:

$$k = \frac{1}{C_K}\cdot\frac{f_l^3}{S_V^2}$$

The Carman-Kozeny constant C_K depends on the structure. The pressure difference due to the Darcy permeability along the infiltration depth x is $\Delta P_{perm}=g_p\cdot x$. Inserting k given by Carman Kozeny in the Darcy law yields:

$$\Delta p_{perm} = g_p\cdot x = \frac{\mu}{k}v_f\cdot x = C_K\cdot\mu\cdot S_L^2\cdot v\cdot x$$

Here $v=\dot{x}=v_f/f_L$ is the velocity of the advancing liquid in the pore volume. With $\Delta p=\Delta p_s+\Delta p_{perm}$ and $2x\dot{x} = {}^{d}/_{dt}\,(x(t)^2)$ integration yields for an infiltration depth $x(t_l)=l$:

$$t_{kc} = \frac{C_K}{2}\cdot\frac{\mu\cdot S_L^2\cdot l^2}{\Delta p-\Delta\sigma\cdot S_L} \qquad (1)$$

For most isotropic structures a Kozeny-constant $C_K=5$ is a good choice [19]. For channels with round cross section one finds $S_L=U_{circ}/A_{circ}=4/d$, applying the Hagen-Poiseuille-equation results in $C_{K,circ}=2$ which reflects a higher permeability along the direction of the channels (but zero in perpendicular directions). For square channels $S_L=4/a$ and $C_{K,sq}\approx 1.78$ [20]. The denominator in equation (1) indicates, that under nonwetting conditions a pressure $\Delta p_{min}=\Delta\sigma\cdot S_L$ has to be exceeded to infiltrate the structure.

3. Discussion

The macrosimulations show, that for finer structures infiltration becomes harder and takes longer, while the phase field simulations show a trend of shorter solidification times for finer structures. For a given set of process and material parameters this results a lower limit for the length scale of structures that can be infiltrated before melt flow is stopped by solidification.

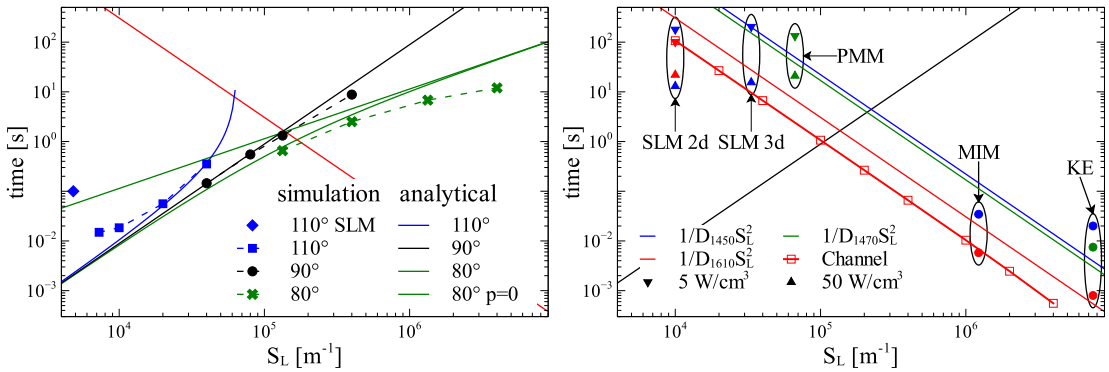

Figure 5: Left: infiltration times, **Right:** solidification times. For better comparability the $1/D_{1610}$-S_L^2 graph is shown with the infiltration times (red, dotted) and the analytical curve for 90° wetting angle with the solidification times (black).

Figure 5 shows infiltration and solidification times side by side, as a measure of (inverse) length scale the specific surface per liquid volume is used. On the left infiltration times for square channels resulting from the macrosimulations are compared to the analytical results for laminar flow through square channels from the previous section for the process and material parameters as discussed above. The numerical results show, that $t \sim S_L^2$ for $\Delta\sigma = 0$ (90° wetting angle), wetting conditions (green) result in faster infiltration and for non wetting conditions (blue) infiltration of finer structures becomes impossible for a given pressure.

The right hand side of figure 5 shows solidification times. As solidification time $t(f_s=95\%)$ is given, since solidification slows down when only small pockets of liquid remain, also a sharp decrease of permeability was observed between 90% and 95% solid fraction. Different melt compositions and starting temperatures are indicated by colour; blue for 25mol%Fe and 1450K, green for 33mol%Fe and 1470K and red for 50mol%Fe and 1610K. Triangles indicate heat extraction of 5 W/cm^3 (up) and 50 W/cm^3 (down), circles indicate isothermal conditions as do squares for the simulations of square channels.

As discussed previously, solidification depends strongly on diffusion in the BCC phase. A dimensional analysis (i.e. application of the Buckingham π theorem) shows that for a process only dependent on diffusion a scaling behaviour $t \sim (D \cdot S_L^2)^{-1}$ should be expected, so the functions $(D_T \cdot S_L^2)^{-1}$ are given as reference as dotted lines. For the coarser SLM and PMM structures the solidification time strongly depends on the heat extraction rate, but for the finer MIM- and KE-structures and isothermal conditions solidification times are governed by structure size. The times for the square channel simulations, which compare the same structure scaled to different sizes, follows the scaling rigidly, the results match $t_{95\%}=(3 \cdot D_{1610} \cdot S_L^2)^{-1}$. It should be noted, that for these simulations due to the high initial Fe- content in the melt no additional intermetallic phases nucleate, so during the solidification the channel shrinks in diameter while the inner melt phase is transformed into the outer BCC phase. At lower initial Fe concentrations in the melt intermetallic phases that form at the solid-liquid interface affect transport of Fe into the melt and hence solidification times.

4. Conclusions

• For non-wetting conditions a certain pressure must be overcome to infiltrate the structures, this pressure is larger for finer structures.

• The simulations show, that wetting conditions (wetting angles < 90°) are beneficial for infiltration. This effect is stronger in finer structures, and can predominate an applied pressure, as was shown for thinner channels or when comparing SLM, to finer PMM and much finer KE structures.
• The diffusivity in the BCC-phase determines how fast Fe can be transported to the solid liquid interface. This strongly affects solidification times, especially for finer structures and leads to short solidification times for fine structures.
• The condition that infiltration should be concluded before permeability is significantly decreased due to solidification limits which structures can be infiltrated under given process conditions (pressure, temperature) and material parameters (wetting conditions, viscosity, diffusivity).

Acknowledgement
This work was performed under project EQUINOX supported by Horizon 2020-European Union, under Grant Agreement No. 689510 and patent application by Kochanek, and co-workers, on EQUINOX manufacturing path is in progress.

References
[1] https://ec.europa.eu/growth/sectors/raw-materials/policy-strategy/sustainable-supply-global_en
[2] https://ec.europa.eu/growth/tools-databases/eip-raw-materials/
[3] https://ec.europa.eu/growth/tools-databases/eip-raw-materials/en/content/strategic-implementation-plan-sip-0
[4] T.B. Sercombe and G. Schaffer: Science 29 Aug 2003, vol. 301, Issue 5637, pp. 1225-1227, DOI: 10.1126/science.1086989
[5] C.T. Liu, E.P. George, P.J. Maziasz, J.H. Schneibel: Mat. Sci. and Eng. A, Vol- 258, Issues 1–2, (1998) pp 84-98, DOI: 10.1016/S0921-5093(98)00921-6
[6] Z. Zhang, D. Jones, S. Yue, P. D. Lee, J. R. Jones, C. J. Sutcliffe and E. Jones: Mat. Sci. Eng. C 33 (7) pp 4055-62 (2013), DOI: 10.1016/j.msec.2013.05.050
[7] Z. Zhang, L. Yuan, P. D. Lee, E. Jones and J. R. Jones: J. Biomed Mater Res B, Nov 2014, VOL 102B (8) pp. 1689-1699, DOI: 10.1002/jbm.b.31804
[8] www.equinox-project.eu
[9] W. Kochanek, US 6939509 METHOD FOR MANUFACTURING METAL PARTS.
[10] https://mdx.plm.automation.siemens.com/star-ccm-plus
[11] MICRESS®, the microstructure evolution simulation software, http://web.micress.de/
[12] Thermocalc Software, www.thermocalc.com, (accessed 1 August 2017).
[13] https://www.thermocalc.com/solutions/by-material/high-entropy-alloys/
[14] B. Böttger, J. Eiken, and M. Apel: Comput. Mater. Sci., 2015, vol. 108, pp. 283–92.
[15] A. Carré, B. Böttger, and M. Apel: J. Cryst. Growth, 2013, vol. 380, pp. 5–13.
[16] Y. Plevachuk, I. Egry, J. Brillo, D. Holland-Moritz and I. Kaban: Int. J. Mater. Res. 2007, 98, 107–111
[17] J. Eiken, B. Böttger, and I. Steinbach: Phys. Rev. E. Stat. Nonlin. Soft Matter Phys., 2006, vol. 73, p. 66122.
[18] M. Eggersmann and H. Mehrer: Philosophical Magazine A, 80:5, (2000) 1219-1244 DOI: 10.1080/01418610008212112
[19] T. Ozgumus, M. Mobedi and U. Ozkol: Engineering Applications of Computational Fluid Mechanics Vol. 8, No. 2, pp. 308–318 (2014)
[20] F. M. White, Fluid Mechanics (McGraw-Hill, 2003)